A ROBOTIC TESTBED FOR LOW-GRAVITY SIMULATION

JAKUB TOMÁŠEK

DIPLOMA THESIS

Czech Technical University in Prague

DIPLOMA THESIS
Jakub Tomášek: *A robotic testbed for low-gravity simulation*

SUPERVISOR:
Jiří Zemánek

Czech Technical University in Prague
Faculty of Electrical Engineering
Department of Control Engineering

© May 2016

ABSTRACT

Upcoming space missions require validation of new robotic concepts for example for on-orbit servicing, active debris removal, and landing on low-gravity bodies. The thesis demonstrates a novel testbed based on a mobile robot for testing in a microgravity and low-gravity environment. When compared to conventional facilities based on air bearings, the testbed allows time-unlimited experiments with significantly lower inertia. The thesis in detail describes development of a prototype as a proof of concept and its verification. The tests demonstrate accurate dynamics at velocities ranging from $20\,\mathrm{mm\,s^{-1}}$ to $200\,\mathrm{mm\,s^{-1}}$ with payload mass of 4.7 kg and support mass of only 2.9 kg. Measured residual acceleration was below $10^{-3}\,g$ but the concept allows to significantly improve this value.

ABSTRAKT

Současné a budoucí vesmírné mise vyžadují testování nových robotických konceptů například pro servisování satelitů, čištění vesmírného smetí a přistávání na vesmírných tělesech s nízkou gravitací. Proto je třeba zreplikovat podobné podmínky na Zemi. Tato práce demonstruje novou platformu pro testování ve stavu bez tíže a ve stavu snížené gravitace. V rámci této práce byl vyvinut prototyp platformy, který byl použit pro validaci tohoto nového konceptu. Testy, které jsou v této práci popsány, ukazují věrohodné chování při plovoucích rychlostech v rozmezí od $20\,\mathrm{mm\,s^{-1}}$ do $200\,\mathrm{mm\,s^{-1}}$. Změřené zbytkové zrychlení bylo pod $10^{-3}\,g$, ale koncept má potenciál přiblížit se ještě více stavu bez tíže. Nová platforma oproti stávajícím technologiím dovoluje testy s nižší hmotností. Přidaná hmotnost k testovanému objektu byla pouze 2.9 kg.

DECLARATION

I hereby declare that this thesis is my own work and effort. Where other sources of information have been used, they have been acknowledged.

Prague, May 2016

Jakub Tomášek

Jakub Tomášek

PROHLÁŠENÍ

Prohlašuji, že jsem předloženou práci vypracoval samostatně a že jsem uvedl veškeré použité informační zdroje v souladu s Metodickým pokynem o dodržování etických principů při přípravě vysokoškolských závěrečných prací.

Praha, Květen 2016

Jakub Tomášek

Jakub Tomášek

ACKNOWLEDGMENTS

The concept realized in this thesis was conceived by Kjetil Wormnes and Gianfranco Visentin from Automation and Robotics Section (TEC-MMA) at European Space Agency (ESA). The work described in this thesis was partly done during my stay at TEC-MMA under guidance of Hendrik Kolvenbach. Hendrik is certainly responsible for the positive outcomes of the work. Marco Pagnamenta contributed in the project with development of a position sensor and with his valuable advices.

Everyone in TEC-MMA was like a family to me. It has been amazing to share my excitement about space exploration and robotics, particularly with Marco Pagnamenta and Rob Hewitt. Besides Hendrik, Marco, Rob, Kjetil, and Gianfranco I want to also mention Evangelos Boukas, Carlos Crespo, and Honza Smíšek and thank everyone for their help, excitement, wisdoms, and friendship.

My great thanks go to Jirka Zemánek for his amazing supervision, round-the-clock curiosity, and help throughout my studies at CTU. Jirka has always been a great inspiration for me with his brilliant ideas, hacks, and projects. On the way I learned many things from him ranging from how to solder to advanced physics. Yet, despite many tries I unfortunately did not manage to master the unicycle.

I just cannot omit Zdeněk Hurák who was my mentor since the very moment I stepped over the doorsill of the AA4CC lab in 2012. He has shaped me as a control engineer and also as a person. I have a great admiration for Zdeněk, and not only because he rides a long board. His knowledge of the field is truly impressive.

CONTENTS

1 INTRODUCTION 1
  1.1 On-orbit servicing 1
  1.2 Active debris removal 2
  1.3 Landing on low-gravity bodies 3
  1.4 Microgravity simulation 4
  1.5 Thesis overview 4
2 GROUND-BASED TESTING IN MICROGRAVITY 5
  2.1 Drop towers and parabolic flights 5
  2.2 Neutral buoyancy pools 6
  2.3 Robotic-arm facilities 7
  2.4 Air-bearing facilities 8
  2.5 Case study of ERA 9
3 A ROBOTIC TESTBED 11
  3.1 Limitations of air-bearing facilities 11
  3.2 From a flat surface to a mobile robot 11
  3.3 Artificial gravity 12
4 PROTOTYPE DEVELOPMENT 15
  4.1 Mobile robot 15
  4.2 Suspension 16
  4.3 Payload 18
  4.4 Pneumatics 18
  4.5 Control system 19
    4.5.1 Payload position measurement 19
    4.5.2 Relative position control 20
    4.5.3 Safety 21
  4.6 Software 21
  4.7 Hardware integration 24
5 VERIFICATION EXPERIMENTS 25
  5.1 Experimental setup 25
  5.2 1D Contact model 25
  5.3 Methods and data 28
  5.4 Discussion 29
    5.4.1 Feedback control 29
    5.4.2 Errors 31
    5.4.3 Limitations 32
6 FUTURE WORK AND CONCLUSIONS 33
  6.1 Future work 33
    6.1.1 Automatic levelling 33
    6.1.2 Omnidirectional wheels 34
  6.2 Conclusions 34
A DIPLOMA THESIS ASSIGNMENT 35

BIBLIOGRAPHY 37

ACRONYMS

AIM	Asteroid Impact Mission
DLR	German Aerospace Center
ERA	European Robotic Arm
ESA	European Space Agency
ESTEC	European Space Research and Technology Centre
GNC	guidance, navigation, and control
GUI	graphical user interface
ISS	Internation Space Station
JAXA	Japan Aerospace Exploration Agency
LEO	Low Earth Orbit
NASA	National Aeronautics and Space Administration
ROOTLESS	Robotic Testbed for Floating-Dynamics Simulation
ROS	Robotic Operating System

1

INTRODUCTION

Space systems are typically associated with exorbitant costs due to the high launch price and the technology development. These systems are often very complex and upon a failure of any critical function the whole project may be lost. Sometimes even astronauts' lives rely on them. Therefore it is crucial to thoroughly test the technologies on the ground.

This is particularly true for robotic systems which are often based on mechanisms and complex algorithms.

Current and future space missions require new robotic technologies and advanced guidance, navigation, and control (GNC). Two trends have recently attracted attention to space robotics: on-orbit servicing and active debris removal. Beyond Earth's orbit, robotics and advanced GNC are also essential in upcoming missions for landing and sampling on low-gravity bodies such as asteroids, comets, and small moons.

1.1 ON-ORBIT SERVICING

Maintanance of space systems includes wide spectrum of tasks such as docking, refuelling, repairing, and upgrading [13]. Several manned servicing missions were performed in the past: for example National Aeronautics and Space Administration (NASA) sent four manned missions to repair Hubble telescope [10].

Manned missions are expensive and dangerous for astronauts. Many of the tasks even cannot be performed by a human. Therefore space agencies and private companies are looking into robotic solutions to protect their assets in space.

A robotic system called Mobile Servicing System has helped to build the ISS and is currently essential for ISS servicing and for other tasks like capturing cargo ships without automatic docking system. It consists of three modular systems [15]: Space Station Remote Manipulator System known as Canadarm2 is a 7-joint serial manipulator 17 m long; Special Purpose Dexterous Manipulator known as Dexter performs delicate maintenance tasks like battery replacement using two 3.3 m-long 7-joint arms and can be attached to Canadarm2 [7]; and Mobile Remote Servicer Base System is a mobile base for the arm. European Space Agency (ESA) has developed its own arm called European Robotic Arm (ERA) and it should be launched to ISS in the near future [5].

Figure 1: Canadarm2 on ISS with anchored astronaut S. Robinson. Photo: NASA.

Mobile Servicing System is operated from a ground control center and saves precious time of astronauts on board of the ISS. They can focus on research instead of spending hours on dangerous extravehicular activities to maintain the station.

On-orbit servicing could significantly extend the lifetime of expensive satellites and even recover satellites from a failure. In the near future, the combination of lower launch costs thanks to reusable rockets and of the autonomous on-orbit servicing could make the Earth orbit more accessible. The technologies for on-orbit servicing must be verified on the ground. More research centres, universities, and private companies will need access to the validation tools and facilities.

1.2 ACTIVE DEBRIS REMOVAL

Currently, in its Cleanspace initiative ESA is focusing on the growing problem of the space debris [37]. At least 5 to 10 objects should be removed every year to sustain the space operations. Otherwise a cascade effect of collisions between the debris and functional satellites will render the Low Earth Orbit (LEO) unusable for the future generations—this effect is also known as Kessler syndrom [18].

One of the main challenges in debris removal is capturing of an uncooperative targets. It has never been done in space before and ESA is developing the technologies to achieve that.

The first mission called e.Deorbit is planned to launch in early 2020s [3]. It is intended to be a technology demonstration and it targets an Earth-observing satellite Envisat. ESA lost control over Envisat in 2012 and the current state is unknown.

Three capture technologies are currently considered [38]: a robotic arm, a tethered net, and a tethered harpoon. ESA has been developing and verifying these technologies in the free-floating environment

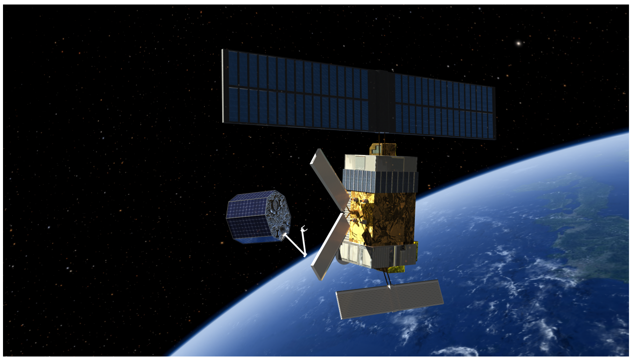

Figure 2: Artist's impression of uncooperative satellite capture using a robotic arm. Image: ESA.

on the ground and in simulations—while there is previous experience with the robotic arms in space, the tethered pull technologies has been studied from the scratch [19]. For instance, [24] describes results of validation of a net simulator in microgravity conditions on a parabolic flight.

To support the verification process, a new facility for orbital robotics and GNC was built at European Space Research and Technology Centre (ESTEC) [20, 21]. It features a flat-floor facility and air-bearing platforms. I supported activities at this facility during my work at ESTEC.

1.3 LANDING ON LOW-GRAVITY BODIES

Recent ESA's very successful mission Rosetta to comet 67P/Churyumov–Gerasimenko [14] put a spacecraft to its orbit and landed on its surface with a lander called Philae in 2014 [2, 34]. While Philae successfully landed on the comet, there were difficulties with the landing gear and Philae bounced off several times before standing still on the surface.

Japan Aerospace Exploration Agency (JAXA) performed successful sample and return mission Hayabusa to asteroid 25143 Itokawa [17]. Part of the spacecraft was a lander Minerva which failed to reach the asteroid.

Despite the success of the missions, they also show the importance of testing and verification. Asteroids are considered to be a major threat for human kind and technologies to deflect them from an impact trajectories with Earth are studied. Further, concepts for asteroid mining are considered [22]. There are planned missions to sample asteroids, for example ESA is preparing Asteroid Impact Mission (AIM) to Didymos asteroids [12]. The spacecraft is planned to carry a lander which should study the surface [11].

1.4 MICROGRAVITY SIMULATION

Both the software and the hardware of the robotic systems must be tested on the ground in an environment similar to the space. Free-floating environment of space is essential for testing of the space robotic systems.

My task was to build a testbed to verify a novel concept for testing in microgravity and low-gravity environment. I built the prototype based on an omnidirectional mobile robot Youbot from Kuka. The testbed was named Robotic Testbed for Floating-Dynamics Simulation (ROOTLESS) and we introduced it in [33]. This thesis describes in detail the development of the testbed.

1.5 THESIS OVERVIEW

Chapter 2 reviews the current state-of-the-art technologies for technology validation in microgravity environment on the ground. Chapter 3 describes the concept of ROOTLESS. As a proof of concept I built a prototype of ROOTLESS—the development including the hardware and software is described in Chapter 4. I participated in cross-validation of the prototype with other types of microgravity testing facilities: Chapter 5 describes the experiments and discusses the performance of the testbed. The outline of the future work is discussed in Chapter 6.

2

GROUND-BASED TESTING IN MICROGRAVITY

Over the years, different methods has been devised to replicate the effects of microgravity on the ground. Often we can limit ourselves to only certain aspects of microgravity to simplify the task. To give a stark example, NASA is putting individuals in tilted beds with head down for extended time period to assess the effects of microgravity on human body [23].

Verification of ongoing and upcoming on-orbit robotic missions requires validation of hardware and GNC algorithms in the free-floating environment. Besides these hardware-in-the-loop tests, we still cannot fully rely on numerical simulations; for instance accurate numerical simulations of contact dynamics in space have not been achieved and we still must rely on real contact.

This section gives an overview of the common methods to emulate microgravity on the ground: drop towers, parabolic flights, zero-buoyancy pools, robotic-arm facilities, and air-bearing facilities. I particularly focus on the description of the air-bearing facilities in Section 2.4 as the concept presented in this thesis builds on and expands on their principle. Also, they are currently the most popular tool for verification of on-orbit technologies [28].

Section 2.5 is a case study of qualification and validation of ERA. It shows how a combination of the described methods was applied.

2.1 DROP TOWERS AND PARABOLIC FLIGHTS

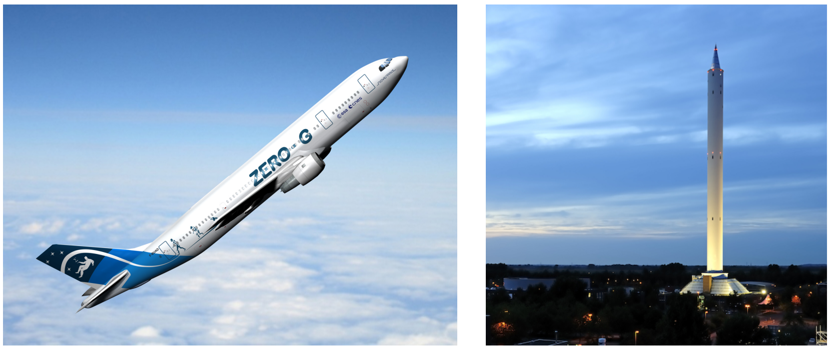

(a) Novespace's Airbus 310 for ZERO-G flights. Photo: Novespace/ESA

(b) The ZARM drop tower in Bremen. Photo: ZARM/University of Bremen

Figure 3: Microgravity facilities exploiting free fall.

An object in orbit is in a free fall. For limited time one can achieve the free fall in drop towers or on parabolic flights for fraction of the price of in-orbit microgravity research for example on ISS.

In drop towers, the experiment is placed in a special capsule which is released untethered from the top of the tower and which falls through an evacuated vertical tube. For example, Fallturm Bremen, a drop tower at University of Bremen, is 122 m high and offers 4.74 s of free fall and diameter of the tube is 3.5 m [16]. At the bottom, the capsule is captured by a special device so the capsule is not damaged. Recently, the facility was upgraded so that the capsule is catapulted from the bottom; this extends the experiment duration to 9.3 s. The fidelity of microgravity reproduction in drop towers is superior to the other methods with residual acceleration ranging from 10^{-6} g to 10^{-3} g.

Parabolic flights achieve longer duration of microgravity; a modified air plane flies along a parabolic trajectory. For example Novespace in France operates Airbus A310 for the parabolic flights in which reasonable microgravity lasts for around 20 s. Residual acceleration is ranging from 10^{-3} g to 10^{-2} g. In a single flight, the parabolic phase is repeated several times.

Parabolic flights and drop towers significantly lower the cost of microgravity research comparing to the cost of performing experiments at ISS. However, the short experiment duration is very limiting. Additionally, the size of the capsule or the space in the plane drive the design of the experiment and can be limiting as well. While parabolic flights are being used for on-orbit technology validation, see for example [24], it is still difficult and impractical to setup and perform the experiments and therefore the cost is still high.

2.2 NEUTRAL BUOYANCY POOLS

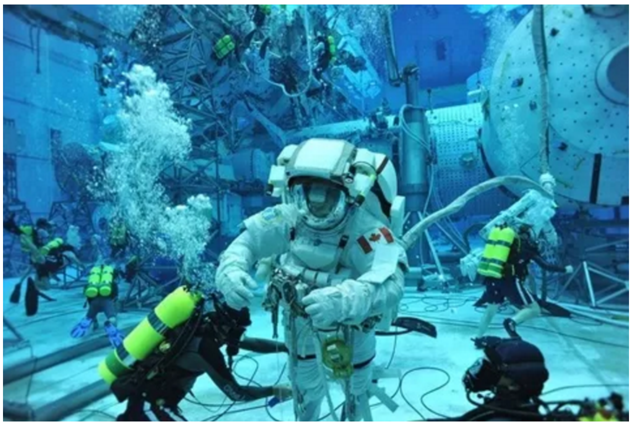

Figure 4: Neutral Buoyancy Laboratory operated by NASA in Houston features a model of ISS for astronaut training. Photo: NASA.

Gravitational force can be compensated by a buoyant force on a submerged object in water. Neutral buoyancy in a pool is achieved by adding special buoyancy control devices. For instance, NASA operates Neutral Buoyancy Laboratory—a 62 m×31 m×13.3 m water tank with submerged model of ISS, see Figure 4.

Neutral buoyancy pools are particularly useful for training astronauts to teach them about body dynamics in the weightless environment. Yet, the drag forces make tests of the robot contact dynamics and of the control in orbit infeasible.

2.3 ROBOTIC-ARM FACILITIES

With maturation of real-time control of robotic-arm manipulators and models of free-floating objects in space, new simulation facilities recently emerged. A scaled mock-up of a free-floating object is attached to a robotic arm. In a feedback loop, the forces on the mock-up are measured by the torque sensors and the model of the free-floating object calculates the arm movement according to the measured forces. Like this, all 6 degrees of freedom are simulated.

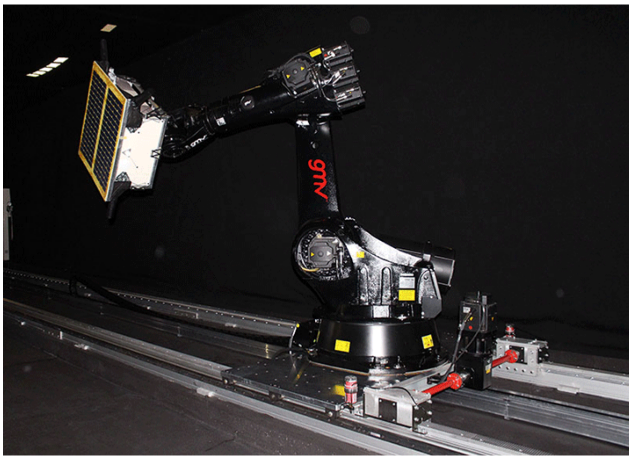

Figure 5: platform-art robotic arm facility developed by GMV. Photo: GMV.

For example, GMV in Spain developed facility called PLATFORM-ART which is currently being used for technology validation for ESA's e.Deorbit and AIM among others [8]; see Figure 5. Other such facilities were built at ESA [30] and at German Aerospace Center (DLR) [1].

These facilities are particularly suitable for contact simulation of on-orbit tasks such as docking and debris removal. As mentioned above, it is hard to accurately numerically model contact dynamics. These facilities use a real contact and rely only on a verified free-floating models.

The concern is however about the fidelity of the feedback loop with delay between measuring the external force and executing the reaction.

2.4 AIR-BEARING FACILITIES

Air-bearing facilities have been used since the beginning of spaceflight for such purposes [31]. They are still the most popular method for verification of on-orbit technologies due to high fidelity comparable to the experiments in the drop towers [28] while being more convenient than the free-fall experiments.

Air bearings use compressed air to create a thin air cushion between two surfaces to minimise friction. Planar air-bearing facilities include extremely flat surface on which a platform with compressed-air container floats using the air bearings. It provides three degrees of freedom: two translational and one rotational. [28] lists 16 air-bearing facilities built at major space research centres but much more are installed around the world.

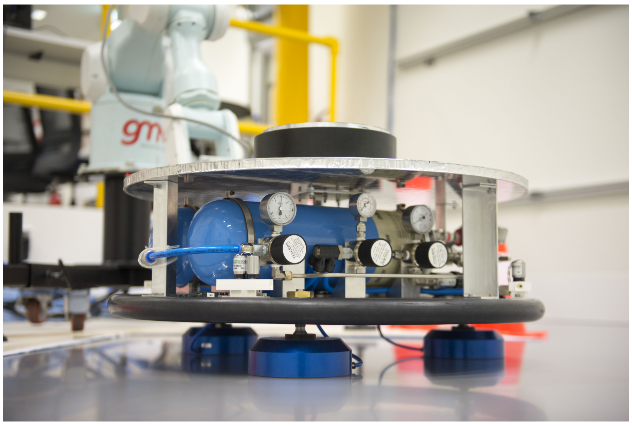

Figure 6: An air-bearing platform on ORBIT flat-floor facility at ESTEC.

A large such facility called ORBIT was constructed as part of the Orbital Robotics and GNC laboratory in 2015 at ESTEC [20, 21]. The facility features floor made of epoxy with area of $45\,\mathrm{m}^2$.

Figure 6 pictures an air-bearing platform on a flat floor. This is a typical setup of such a platform: at the bottom there are three air bearings pointing down, in the middle there is pneumatic system with pressurized-air tank, and an interface mockup of a satellite is mounted at the top.

The planar platforms can be further extended to 5 degrees of freedom by adding a spherical air bearing on top of the platform. Even 6 degrees of freedom air-bearing platforms has been reported. For example in [29], the platform adds the 6th degree of freedom by adding a pulley system with counter weight to compensate the gravitational force.

Air-bearing facilities and robotic-arm facilities complement each other. The advantage comparing to robotic-arm simulation is that air-bearing facilities can be considered the ground truth for contact forces. The results from air bearing facilities can be then used to improve the numerical model used for control in the robotic-arm facilities with 6 degrees of freedom [26].

2.5 CASE STUDY OF ERA

ERA is a robotic arm developed for ISS by ESA and ROSCOSMOS [9]. After several postponements ERA is now bound to launch together with a new Russian ISS module called Nauka or Multipurpose Laboratory Module in 2017.

ERA is in design similar to currently operating Canadarm2 mentioned above—it is a symmetric 7-joint manipulator 11.3 m long. Compared to Canadarm2, ERA is compatible with the Russian segment of the ISS and it has more autonomy.

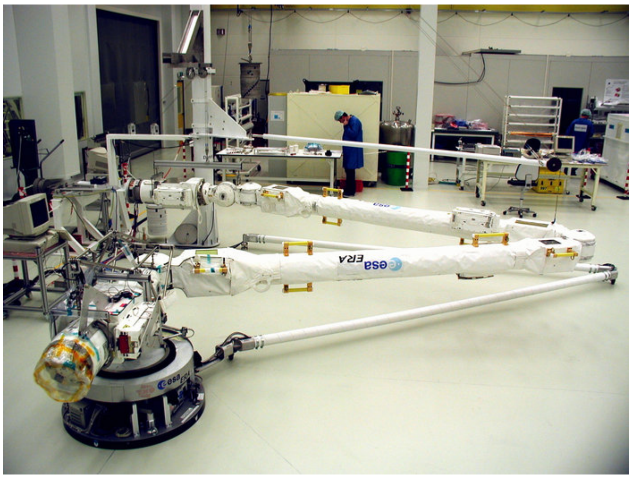

Figure 7: ERA during flat-floor testing at a test facility specifically designed for ERA. The tip of ERA is supported by an air bearing. Photo: Dutch Space, ESA.

ERA went through qualification and thorough testing [36]. The tests included performance and function tests of the electrical subsystems, mechanical subsystems, control system, and autonomy features. For that, a special flat-floor facility was designed by Dutch Space to simulate the free-floating environment [35], see Figure 7. The tip of the arm is supported by an air bearing and the weight of the extended arm is supported by a pulley system to release torque from the joints.

Also, operations and hardware repair procedures in microgravity were tested with an ESA astronaut submerged in neutral-buoyancy pool in Gagarin Cosmonaut Training center [32].

3

A ROBOTIC TESTBED

3.1 LIMITATIONS OF AIR-BEARING FACILITIES

Air-bearing facilities have several issues.

Firstly, the object under test (below referred to as *payload*) must be mounted on an air-bearing platform. The platform has its own air and energy supply in order not to suffer from external forces and torques from the connected air hoses and electrical cables. Therefore the duration of the experiments is limited by the energy and air storage.

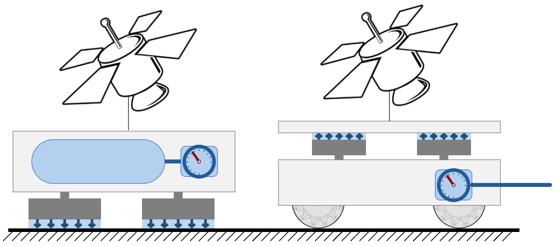

Figure 8: Illustration of difference between a conventional air-bearing platform (left) and ROOTLESS (right).

Moreover, by placing the payload on such a platform, the inertia of the platform combines with that of the payload. This must be taken into account in the payload design and in the numerical model.

Secondly, the flat surface limits the maximum distance the platforms can operate over. Installing and maintaining a permanent flat surface for experiments is expensive and may be impractical for universities and smaller research facilities.

A typical air-bearing platform is illustrated in Figure 8.

3.2 FROM A FLAT SURFACE TO A MOBILE ROBOT

ROOTLESS overcomes the limitations mentioned above.

Similarly to conventional air-bearing facilities, the concept is based on air bearings to provide low-friction movement in the horizontal plane. Instead of pointing down mounted to the payload through a platform, three or more air bearings are mounted on a mobile robot pointing upwards as Figure 8 illustrates. The payload is mounted on a flat plate that floats on a thin air film on top of the air bearings. As the payload moves the mobile robot follows it respectively using the information about the horizontal distance between the mobile robot and the payload from a contactless sensor.

Like this, the platform can be permanently connected by air hose without disturbing the payload. The experiments are therefore not limited neither in duration by the size of the pressured-air tank nor in the distance by the limited size of a flat floor.

Moreover, ultimately a flat surface itself is not necessary. And finally, only a simple light interface plate is mounted to the payload introducing small uncertainty in the model and allowing lower-mass experiments. Figure 8 illustrates the differences between a conventional air-bearing platform and the proposed testbed.

3.3 ARTIFICIAL GRAVITY

Additionally to the mentioned advantages, an artificial gravitational force can be introduced on the payload by tilting the horizontal plane in which the payload floats. Tilting involves precisely adjusting the height of the air bearings and can be used for the test and validation of robotic systems on low-gravity objects such as asteroids, comets, and small moons.

Table 1 lists low-gravity bodies interesting for the simulation with ROOTLESS. For practical reasons and due to the velocity limits of the robot it is feasible to emulate gravitational acceleration below $0.1\,\mathrm{m\,s^{-2}}$.

If the free-floating plane is tilted and the robot accelerates, there is an additional undesired force acting upon the payload besides the gravity. Below I try to show that for the small simulated acceleration, the acceleration of the robot has only a negligible effect on the payload.

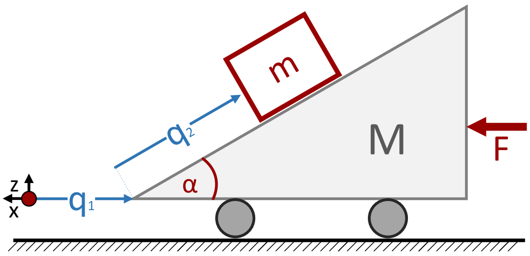

Figure 9: Modelling an artificial gravity as a moving inclined plane. I assume zero friction. I define coordinates q_1 and q_2.

The situation can be simplified to accelerating inclined plane as illustrated in Figure 9. I consider the case when the inclined plane with mass M is accelerating in x direction. The payload, a box with mass

m, is placed on the inclined plane sliding with zero friction. I used Euler-Lagrange equation to derive the acceleration of the payload:

$$\begin{aligned} \ddot{q}_1 &= \frac{2F + mg\sin 2\alpha}{2M + 2m\sin^2\alpha}, \\ \ddot{q}_2 &= -\frac{g(m+M)\sin\alpha + F\cos\alpha}{M + m\sin^2\alpha}, \end{aligned} \tag{1}$$

where q_1 and q_2 are generalized coordinates defined in Figure 9, α is the angle of the inclined plane, m and M are respectively the mass of the payload and of the incline, g is the gravitational constant, and F is the force pushing the incline. I am interested in acceleration of the payload in x direction; I rewrite Equation 1 using $\ddot{x} = \ddot{q}_1 + \ddot{q}_2 \cos\alpha$:

$$\ddot{x} = \frac{\sin^2\alpha}{\frac{m}{M}\sin^2\alpha + 1} a + \frac{\sin\alpha\cos\alpha}{\frac{m}{M}\sin^2\alpha + 1} g = Aa + Bg. \tag{2}$$

a is acceleration of the robot. The payload acceleration clearly splits into two terms where the first term is caused by acceleration of the robot and the second term by gravitation. The ratio of the terms is

$$r = \frac{A}{B} = \tan\alpha.$$

Table 1: Approximate gravitational acceleration at surface of interesting low-gravity bodies.

BODY	g $[\mathrm{m\,s^{-2}}]$	$\alpha\,[°]$
Ceres	0.2845	1.6618
Hygiea	0.091	0.533
Lutetia	0.05	0.292
Phobos	0.0057	0.033
67P	10^{-3}	0.006
25143 Itokawa	10^{-4}	0.0006

For low acceleration the angle α is small and the maximum value of the ratio $r = 0.01$. Additionally, the typical acceleration a is at least an order smaller than g. Therefore, $Aa \ll Bg$ and the effects of accelerating robot on the movement of the payload are negligible.

4

PROTOTYPE DEVELOPMENT

I built a prototype of the testbed. There were five function requirements for the platform:

- unconstrained planar movement,
- decouple the robotic platform from the payload,
- provide safe operation,
- allow moving over common floors,
- and recreate artificial gravity scenarios.

In this first iteration the focus was on testing the first three functions—free-floating payload on top of a mobile robot—but during the design it was necessary to take into account all the points for easy upgrades in the future.

The prototype integrates five core subsystems: a mobile robot, suspension, payload, pneumatic system, and control system. The control system includes the computer and software. Figure 10 gives the system overview and illustrates how the hardware subsystems are integrated. All the subsystems are discussed below in detail.

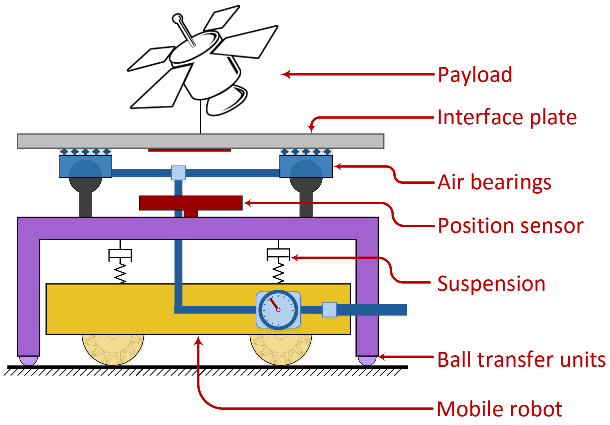

Figure 10: System overview.

4.1 MOBILE ROBOT

The prototype is based on Youbot from Kuka. Youbot is a commercially-available holonomic mobile robot widely used by academic researchers

[4]. Figure 11 shows the robot. This solution allowed to benefit from the community during the development, to shorten the development time, and to lower the total cost.

The core requirement was the unconstrained planar locomotion. Youbot is equipped with mecanum wheels so the robot can move in any direction from any configuration. Each wheel is propelled by an independent motor controlled by Trinamic TMCM controller. The motors are connected to an onboard computer with Intel Atom Dual-Core central processing unit. Besides that, it features power system with a battery providing up to 1 h of operation. It was not necessary to use the battery as the robot can be powered all the time.

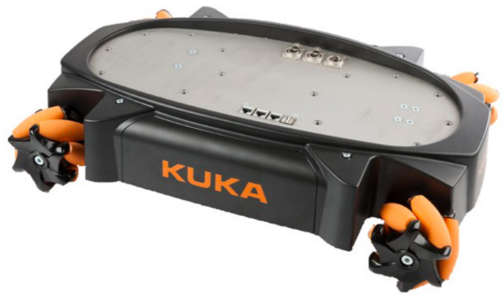

Figure 11: Youbot from Kuka. It provides unconstrained planar movement with the use of mecanum wheels.

Mecanum wheels feature series of rollers mounted at 45° angle around its circumference. By rotating each wheel with different computed velocity one can move in any direction. The maximum velocity in the forward direction of the robot is $0.8\,\mathrm{m\,s^{-1}}$.

4.2 SUSPENSION

The drawback of the mecanum wheels is the discontinuous point of contact with the ground. There is a gap between each roller and as the wheel rotates the rollers collide with the ground. This motion introduces significant vertical vibrations to the robot and may disturb the motion of the payload. Figure 12 shows the vibrations measured on top of the robot and its frequency spectrum. The vibrations peak at frequency 30 Hz.

The vibrations are intolerable for the simulation of microgravity. In order to damp the vibrations, I built a frame around the Youbot which carries the air bearings and the payload. The frame is made of aluminium profiles. The weight of the frame and payload is supported by ball transfer units which allow holonomic movement with small rolling resistance.

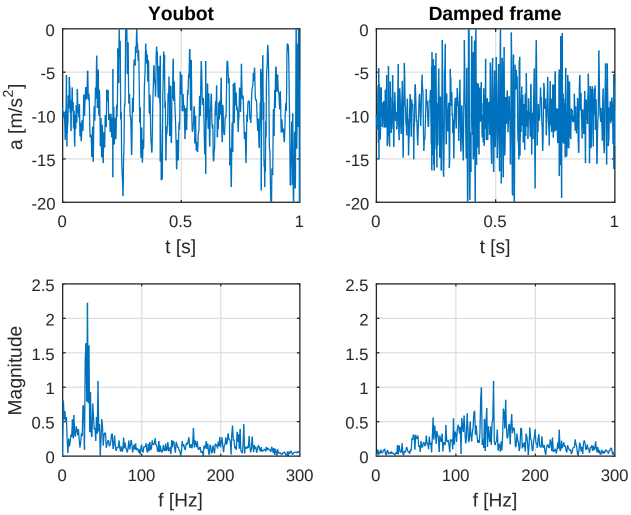

Figure 12: Vibrations on top of the Youbot (top left) and on top of a damped frame (top right) with a payload of 8 kg measured by accelerometer. The robot moved in forward direction with velocity $0.8\,\mathrm{m\,s^{-1}}$. The frequency spectrum of the signal (bottom) shows that the peak frequency around 30 Hz on the Youbot was damped. New vibrations with higher frequency are introduced from the ball transfer units.

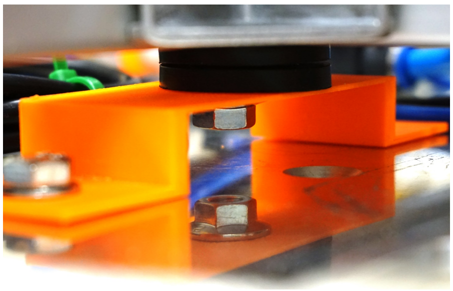

Figure 13: Spring-damper system to damp vertical vibrations introduced by mecanum wheels.

A spring-damper system damps the vertical vibrations from the robot. This system consists of three 3D-printed brackets from PLA with a rubber acting as a spring attached between the robot and the frame at three points along the axis; see Figure 13. I tuned the effect of suspension by altering the thickness of the bracket.

This proved to be sufficient to minimise the vertical vibrations. Figure 12 compares the vibrations measured on top of Youbot and on top of the damped frame. The vibration peaks in low frequency were completely removed. New vibrations with higher frequency were introduced from the rollers inside the ball transfer units. These vibrations were however tolerable.

4.3 PAYLOAD

The air gap between the air bearings and the payload is only a few micrometers thick. Therefore it is crucial that the interface surface between the payload and the air bearings is flat and smooth, or else the surfaces could come in contact. Additionally, the flat material must be stiff, so as not to deform when a heavier payload is used. The material should also be light, so as not to constrain the minimum mass of the whole payload.

I tested several interface materials: aluminum, acrylic, and glass. Glass, while being delicate to handle, has the best floating properties. As the interface material I opted for an off-the-shelf circular mirror with a diameter of 40 cm and a thickness of 5 mm.

I attached the mirror to a 10 mm-thick honeycomb panel with equidistant M6 inserts to provide a generic and easy-to-use mounting interface for different payloads. The honeycomb panel is light and increases stiffness so heavier payload can be used without the risk of breaking the mirror. The total weight of the interface plate is 2.94 kg. The plate can be seen in Figure 21 on top of ROOTLESS.

The honeycomb panel we purchased had large cells of the honeycomb structure and therefore lots of glue had to be used to fix the inserts. The amount of glue unnecessarily increases the weight of the interface plate.

The interface plate is the only addition to the payload. Because the interface plate is symmetrical it is easy to include it in the simulation model of the whole payload. Unlike bulky platforms with pneumatic systems in conventional air-bearing facilities, it does not introduce any uncertainty in the model. For example, the platform in Figure 6 weighs more than 27 kg. In fact the weight could be significantly reduced with an interface plate designed specially for the payload without any generic mounting.

4.4 PNEUMATICS

To provide low-friction connection for the floating payload in plane air bearings were chosen. An air bearing is a type of a bearing which uses pressurized air to create a thin air film to eliminate friction between two surfaces. When an air bearing is working properly, there is no contact between the two surfaces so there is zero friction; however drag force of the air still remains.

I mounted three New Way air-bearing pucks shown in Figure 14 on top of the suspended frame with ball mounting screws. The ball allows the air bearings to freely tilt in roll, pitch, and yaw so when a flat surface is placed on top, all the three air bearings properly align with the surface.

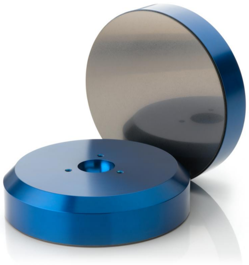

Figure 14: New Way air bearings.

The pneumatic system provides clean air with constant pressure. Figure 15 shows the diagram of the pneumatic system. The pressurized air is provided externally. Not to clog the pores of the air bearings, the air is at first filtered from small particles and liquid drops. Then, the pressure of the air is regulated. In experiments, 2 bar was sufficient pressure for payload with weight of around 7 kg.

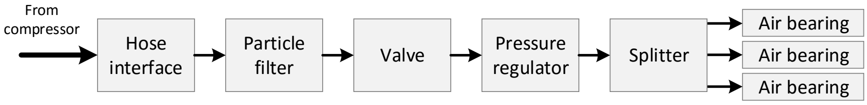

Figure 15: Pneumatics diagram.

4.5 CONTROL SYSTEM

The center of mass of the payload must remain within the area between the air bearings. Otherwise the payload tips over and falls. As the payload moves Youbot follows it using feedback control algorithm running on the onboard computer with information about the distance between the payload and the mobile robot.

4.5.1 *Payload position measurement*

A custom vision-based sensor was developed specifically for the task of measuring the absolute distance between the payload and the robot. It is based on tracking a target on the interface plate. The sensor was devised and developed by my colleague Marco Pagnamenta. I implemented the algorithm to process the raw data from the sensor in Beaglebone Black microcomputer.

A circular dark target is attached to the bottom of the interface plate. Three line CCD cameras capture the position of the edges of the circle. They are attached to the damped frame close to the interface plate. The sensor is placed close not to be affected by the ambient light. LEDs along the line cameras provide lighting. Figure 16 shows the sensor in a 3D printed package.

The used line CCD sensor was TSL2014 with size of pixel 0.127 mm and active length 112 mm. The diameter of the target is 80 mm.

Beaglebone Black Board is a microcomputer running Debian; it is suitable for embedded applications and rapid prototyping. The data from the CCD cameras are processed by Beaglebone Black Board with frequency 2 kHz. The data are filtered down to frequency 30 Hz which is reasonable for Robotic Operating System (ROS).

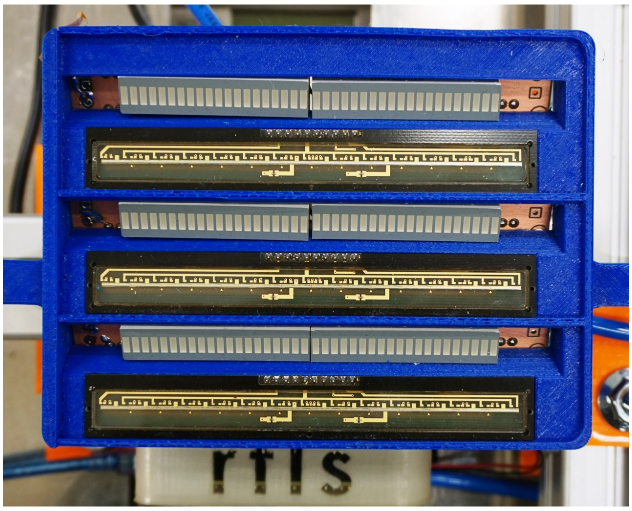

Figure 16: Custom sensor for measuring the relative position between the payload and Youbot.

I implemented the algorithm for circle position estimation in C. I tested several methods for estimation. For instance I tried to use least square fitting of the edge points with a circle. It turned out that the available number of points on the circle for this method is too low and the output was unstable. Finally, the algorithm at first calculates intersection of two circles with center at edge points and the radius of the target between all pairs of the edge points. The algorithm clusters the intersections and the cluster with the most points is considered to be the center. The center is computed as the average of the points. When only two edge points are detected, the center is the point closest to the solution in the previous step. Together with the averaging, the output of the sensor is smooth and stable.

4.5.2 *Relative position control*

Figure 19 shows the feedback loop for the relative position control. The interface plate is circular so only the translation degrees of freedom, i.e. x and y position, are measured and controlled. The raw payload-position data from the sensor are processed by a Beaglebone Black microcomputer. The Beaglebone Black Board feeds the position information to the onboard computer through RS485. The feedback loop is closed through a PID controller running on the onboard computer and commands the velocity vector of the platform, for more details see Section 4.6 describing software of the platform.

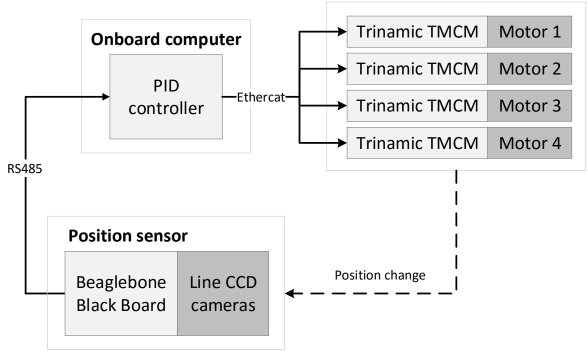
Onboard computer
PID controller
Ethercat
Trinamic TMCM
Motor 1
Trinamic TMCM
Motor 2
Trinamic TMCM
Motor 3
Trinamic TMCM
Motor 4
RS485
Position sensor
Beaglebone Black Board
Line CCD cameras
Position change

Figure 17: Relative position control loop.

The velocity commands for the Youbot are then converted into angular-velocity commands for each motor. The four independent motors are controlled by Trinamic TMCM motor controllers which are connected with the onboard computer via Ethercat.

4.5.3 *Safety*

I added a hard stop button which disables the power of the motors when pressed. The tracking is enabled only when the sensor detects the circular target. If the payload is removed, the robot stops the operation.

Two Hokuyo laser scanners are mounted on the testbed to provide safe operation of the robot. It functions as a soft stop. When an unexpected obstacle is detected, the robot stops the operation and waits for the operator.

I added bumpers to protect the payload from sliding down from the air bearings.

4.6 SOFTWARE

The onboard computer runs Ubuntu. ROS was chosen as the robotic framework for the software development as the drivers for the platform itself already exist [27]. Over past few years, ROS has become a standard tool for robotic systems. It significantly simplifies the software development. Figure 18 shows a simplified diagram of the ROS nodes. I implemented all the ROS nodes in Python.

ROS master is running on the onboard computer while there is control station connected over wifi network. Additionally, a joypad is connected over an RF connection to Youbot as a remote control.

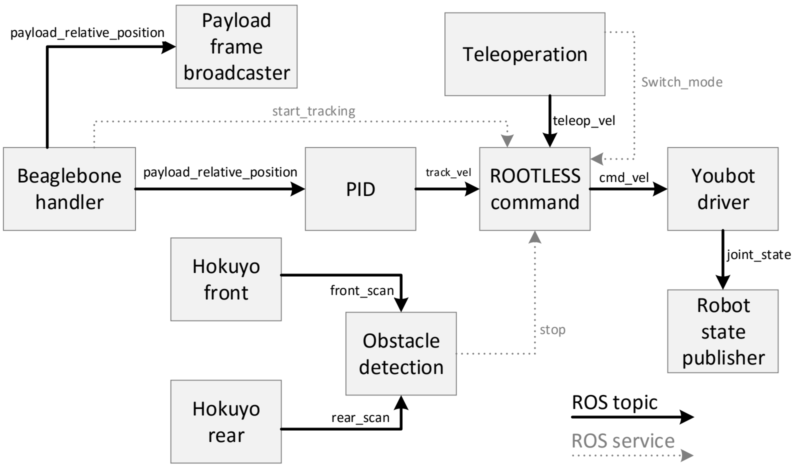
payload_relative_position
Payload frame broadcaster
Teleoperation
Switch_mode
start_tracking
teleop_vel
Beaglebone handler
payload_relative_position
PID
track_vel
ROOTLESS command
cmd_vel
Youbot driver
joint_state
Hokuyo front
front_scan
Obstacle detection
stop
Robot state publisher
Hokuyo rear
rear_scan
ROS topic
ROS service

Figure 18: Simplified diagram of ROS nodes, topics, and services.

There are two modes of operation of the testbed: a tracking mode and a teleoperation mode. In the latter, the robot can be remotely controlled using a joypad. In the tracking mode, when a payload with a target is placed above the robot, the robot moves according to the movement of the payload and tries to keep the distance minimal.

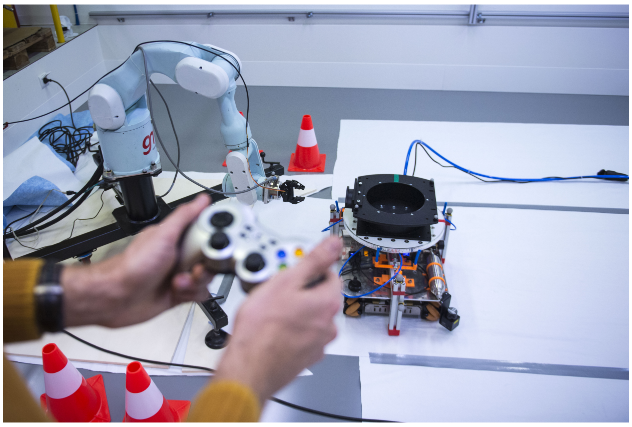

Figure 19: Joypad is used to operate the testbed during experiments.

I implemented a simple PID controller which runs with constant frequency 30 Hz. The output of the PID controller node are velocity commands in x and y. ROOTLESS command node forwards either the teleoperation or tracking commands to the Youbot driver. Youbot driver recomputes the Cartesian velocity commands to angular commands of each motor.

I prepared a simple GUI based on RQT and RVIZ which runs in the control station, see Figure 20. It allows the operator to inspect the status of the robot and change modes and parameters, for example the operator can change the gains of the PID controller on the fly.

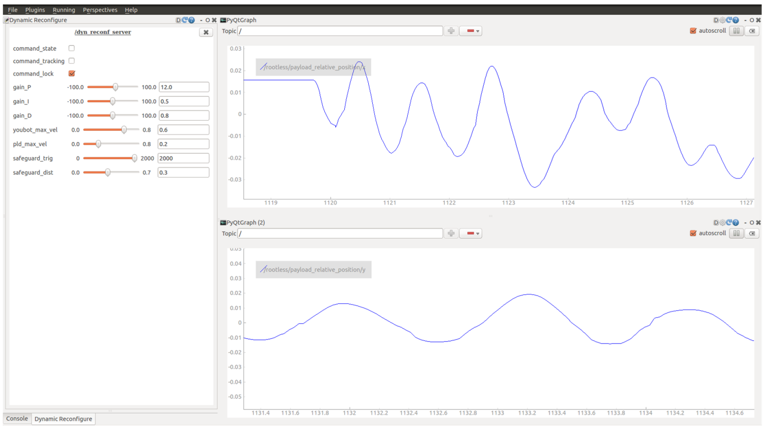
File
Plugins
Running
Perspectives
Help
Dynamic Reconfigure
PyQtGraph
PyQtGraph (2)
Topic /
autoscroll
/rootless/payload_relative_position/x
/rootless/payload_relative_position/y
Console
Dynamic Reconfigure

/dyn_reconf_server

command_state ☐
command_tracking ☐
command_lock ☑
gain_P -100.0 100.0 12.0
gain_I -100.0 100.0 0.5
gain_D -100.0 100.0 0.8
youbot_max_vel 0.0 0.8 0.6
pld_max_vel 0.0 0.8 0.2
safeguard_trig 0 2000 2000
safeguard_dist 0.0 0.7 0.3

(a) GUI based on RQT.

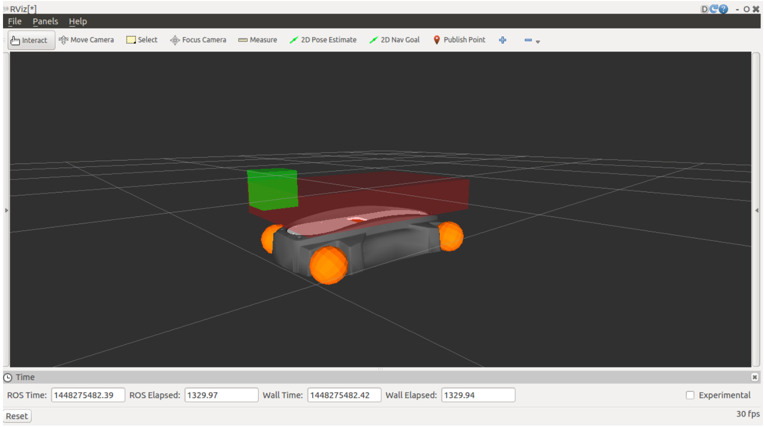
RViz[*]
File
Panels
Help
Interact
Move Camera
Select
Focus Camera
Measure
2D Pose Estimate
2D Nav Goal
Publish Point
Time
Reset
30 fps

ROS Time: 1448275482.39 ROS Elapsed: 1329.97 Wall Time: 1448275482.42 Wall Elapsed: 1329.94 ☐ Experimental

(b) Robot state in RVIZ. Red box visualizes the payload with green box showing the orientation.

Figure 20: GUI to operate the testbed.

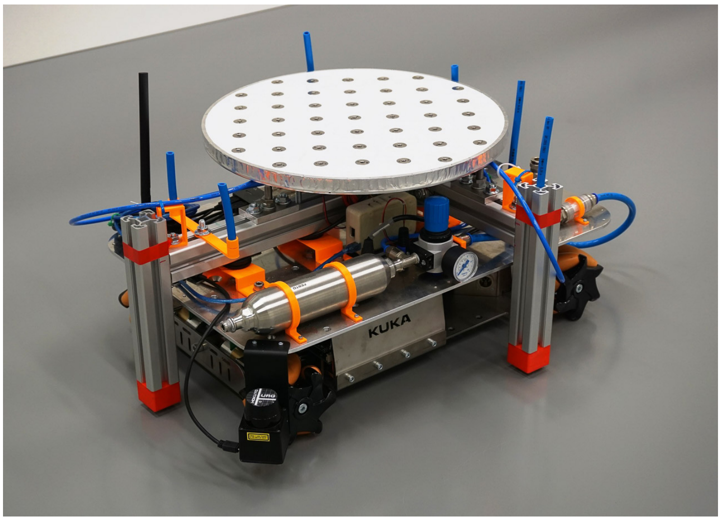

Figure 21: Final prototype of ROOTLESS.

The reconfiguration on the fly is performed via Dynamic Reconfigure Server. The same configurations can be set with the joypad.

4.7 HARDWARE INTEGRATION

Figure 21 shows the final version of the testbed prototype. I used 3D printing and Velcro for the mechanical integration.

5

VERIFICATION EXPERIMENTS

5.1 EXPERIMENTAL SETUP

Experiments emulated a contact between a chaser approaching a target in orbit.

A robotic arm Mitsubishi PA10 approached a target on a predefined linear trajectory with different approach velocities. The target—a simple cylinder with diameter 300 mm—was the payload of ROOTLESS, i.e. it was attached to the payload plate and free floating on top of the platform. The goal of the experiments was to measure the free-floating trajectory of the payload and compare it to the expected trajectory and velocity. Figure 22 illustrates the setup of the experiments and Figure 23 shows actual image of the experimental setup.

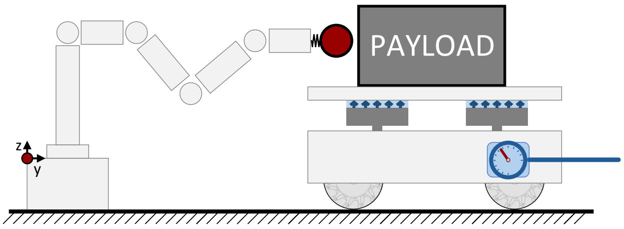

Figure 22: Illustration of experiment setup.

We performed the experiments on ORBIT flat-floor facility. It is equipped with Vicon motion capture system which allowed to measure the positions with sampling rate of 250 Hz and with accuracy below 1 mm. Position of the payload, of the robotic arm, and of the platform were tracked. There was a foil on the floor to protect the floor from impacts of the mecanum wheels.

The experiments were performed as part of the cross validation of the ORBIT flat-floor facility with PLATFORM-ART—robotic-arm simulation facility developed by GMV. A more detailed description and data analysis of the experiments can be found in [26]. I performed the ROOTLESS experiments together with my colleague Hendrik Kolvenbach and with Andrea Pellicani from GMV.

5.2 1D CONTACT MODEL

To verify the system a simple, predictable, and measurable contact was designed. To closely emulate only a point contact the interface of

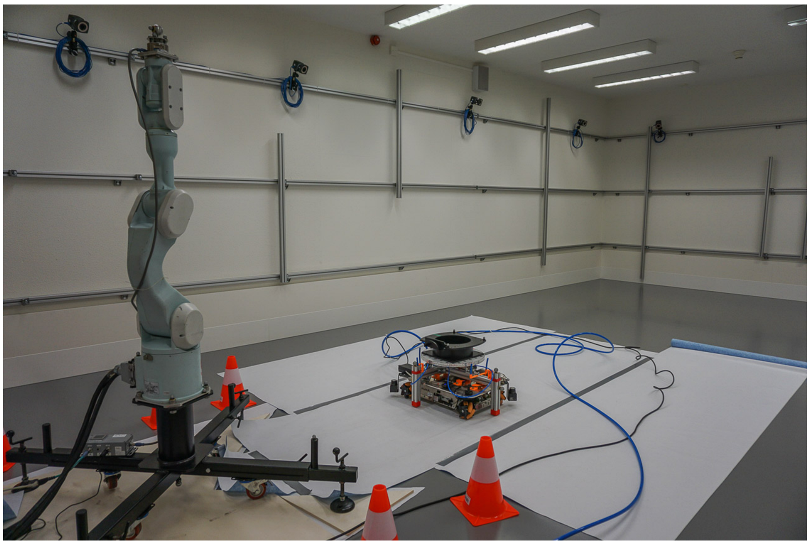

Figure 23: Setup of the experiments carried out on the ORBIT flat-floor facility with Vicon motion capture system. On the left can be seen Mitsubishi PA10 robotic arm used to impact the payload and in the center ROOTLESS with a mockup of a satellite launch adapter ring as payload.

the contact on the side of the robotic arm was a sphere and the target was a cylinder; Figure 24 shows the end-effector.

A known compliance device, a spring-damper system, was placed behind the contact interface on the robotic arm. This allows to neglect other deformations and simply model the deformation as a spring. Like this, the results can be compared to simulation[1].

The chaser is approaching the target with a constant velocity v_0. During the contact, the system behaves as a spring damper system. We can simplify the problem to one dimension. The spring damper system can be modelled as a damped oscillator:

$$\ddot{x} + \frac{b}{m}\dot{x} + \frac{k}{m}x = 0$$

where b is damping and k is the spring constant. I set the point of contact at time $t = t_c = 0$ to $x(0) = 0$. In the reference frame of the chaser, the initial velocity is $\dot{x}(0) = -v_0$. The response to these initial conditions is:

$$x(t) = \frac{v_0 m}{\sqrt{b^2 - 4\,k\,m}} \left(\mathrm{e}^{-\frac{b+\sqrt{b^2-4\,k\,m}}{2\,m}\,t} - \mathrm{e}^{-\frac{b-\sqrt{b^2-4\,k\,m}}{2\,m}\,t} \right).$$

The payload is released when the velocity reaches its first peak. I determine the time of release t_r by finding the extreme of $\dot{x}$:

$$t_r = \frac{m\,\left(\log\left(-\frac{b\,\sqrt{b^2-4\,k\,m}-2\,k\,m+b^2}{2\,k\,m+b\,\sqrt{b^2-4\,k\,m}-b^2}\right)+2\,\pi\,\mathrm{i}\right)}{\sqrt{b^2-4\,k\,m}}$$

---

[1] Typically, the function of the testbed is opposite—the experiments should be taken as the reference for the simulation.

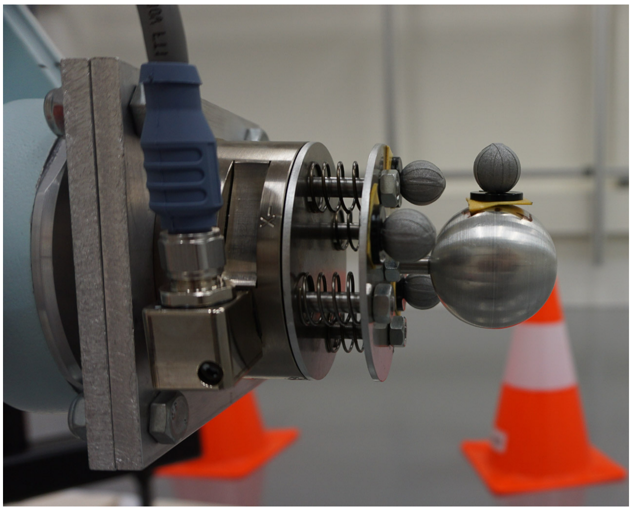

Figure 24: The robotic arm end effector used in the experiments. From left: load cell, compliance device, contact interface. Spherical targets are attached for Vicon motion capture.

where log is natural logarithm and i is imaginary unit. Now, the velocity of release v_r in the global coordinate frame is then explicitly expressed:

$$
\begin{aligned}
v_r &= v_0 + \frac{v_0}{2}\,(A-1)\,\mathrm{e}^{-\frac{B}{2}(A-1)} - \frac{v_0}{2}\,(A+1)\,\mathrm{e}^{-\frac{B}{2}(A+1)} \\
A &= \frac{b}{\sqrt{b^2-4\,k\,m}}, \\
B &= \log\left(-\frac{b\sqrt{b^2-4\,k\,m}-2\,k\,m+b^2}{2\,k\,m+b\sqrt{b^2-4\,k\,m}-b^2}\right)+2\,\pi\,\mathrm{i}.
\end{aligned}
\tag{3}
$$

For the undamped system, i.e. $b = 0$, the velocity at release simplifies to $v_r = 2\,v_0$. After the release, the payload continues to move without energy dissipation and thus with constant velocity v_r. The model in the global coordinate frame is summarized as:

$$
\begin{aligned}
t \in \langle 0, t_r\rangle \implies x(t) &= x_1\,(t) = \mathrm{v}_0\,t+ \\
&+\frac{v_0 m}{\sqrt{b^2-4\,k\,m}}\left(\mathrm{e}^{-\frac{b+\sqrt{b^2-4\,k\,m}}{2\,m}\,t}-\mathrm{e}^{-\frac{b-\sqrt{b^2-4\,k\,m}}{2\,m}\,t}\right), \\
t > t_r \implies x(t) &= x_1(t_r) + v_r\,(t-t_r)\,.
\end{aligned}
\tag{4}
$$

The springs were designed to have $k = 1000\,\mathrm{N\,m^{-1}}$ and payload with the attached interface plate had $m = 7.64\,\mathrm{kg}$. Damping was low but non negligible.

5.3 METHODS AND DATA

We performed impacts with relative velocities of 10 mm s^{-1}, 30 mm s^{-1}, 50 mm s^{-1}, and 100 mm s^{-1}. Each experiment was repeated several times.

The main source of the data shown here is the Vicon motion tracking system. However, I also used the data from a load cell which was installed at the tip of the robotic arm to measure the contact forces and torques. Also, the data from the on-board position sensor and Youbot's odometric system are taken into account in the analysis.

In results I compare only the measured trajectory to the model after the impact. For analysis of the impact please refer to [26].

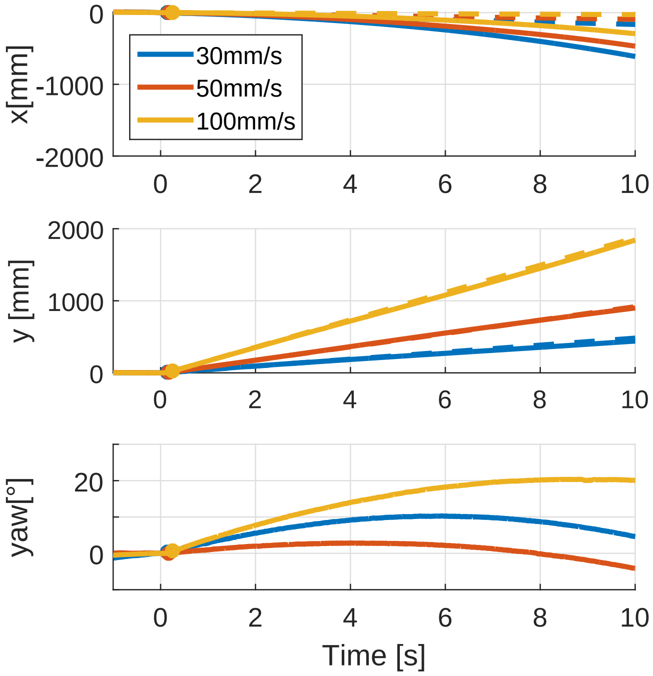

Figure 25: Trajectory comparison after contact with different approach velocities in y direction. The dashed line shows the expected trajectory after contact without any external disturbance.

Figure 25 displays a sample of a trajectories of a free-floating satellite during the experiment for each velocity. Figure 26 then focuses on the experiments with approach velocity 50 mm s^{-1} to show the repeatability. The data were similar to experiments with other velocities.

Figure 27 compares the position of the payload and the robot during the initial phase of the contact experiment with approach velocity of 50 mm s^{-1}. It shows how the feedback controller tracks the floating payload. One can notice reaction delay to the initial movement of the payload of approximately 0.15 s. After 0.5 s the robot accelerates to the velocity of the payload. The errors, like slipping of the wheels,

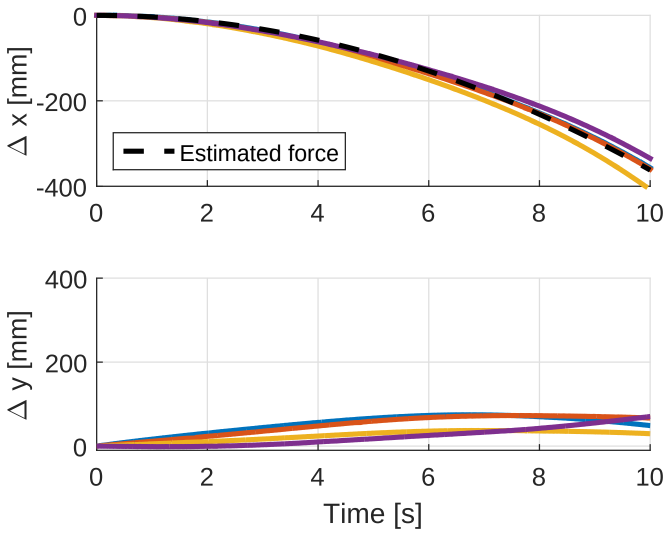

Figure 26: Error between expected position and real position after floating payload release for repeated contact experiments with approach velocity $50\,\mathrm{mm\,s^{-1}}$. The dashed line shows estimated constant acceleration caused by inclination of the floating plane.

are corrected by the feedback controller, which results in oscillations along the trajectory of the robot.

Figure 28 gives more detailed look at the controller performance. It shows a step response and tracking of accelerating payload. Also it compares the measurements from the on-board sensor with the motion tracking measurements.

5.4 DISCUSSION

I performed only a simple experiment to verify the testbed. While more thorough testing must be done in the future to estimate the residual acceleration, the results are promising. Looking back it would be useful to place an accelerometer in the payload.

5.4.1 *Feedback control*

I measured the delay in the feedback loop to be around 12 ms. Due to the architecture of the system the delay was variable. Overall position reaction was even longer due to the neglected dynamics of the motors.

Despite the delay, the PID control was sufficient under the conditions of the experiments. For accelerating payload in Figure 28 the error increases over the time as I gain was set low. The preference was put on the fast response to the abrupt changes during the contacts.

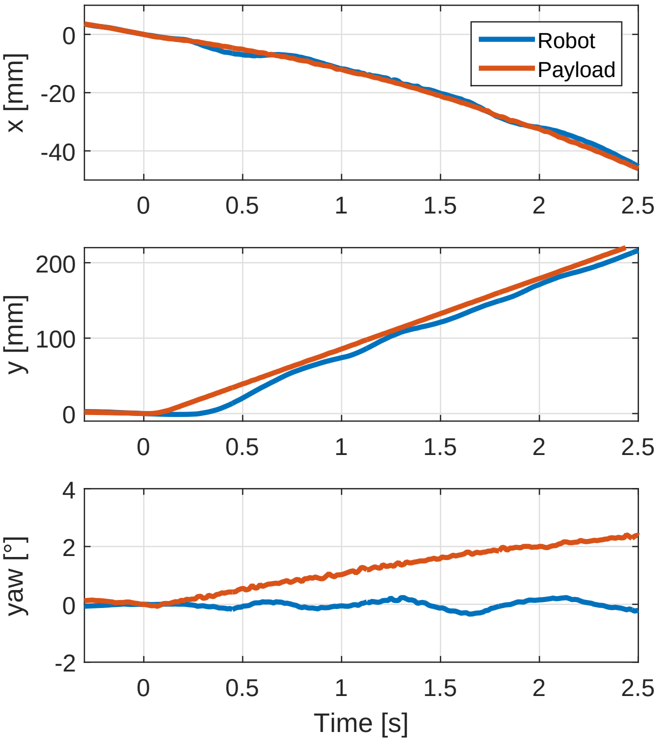

Figure 27: Trajectory of payload and robot during the simple contact experiment with approach velocity 50 mm s^{-1}. Time of contact between the chaser and the payload was at $t_c = 0$ s.

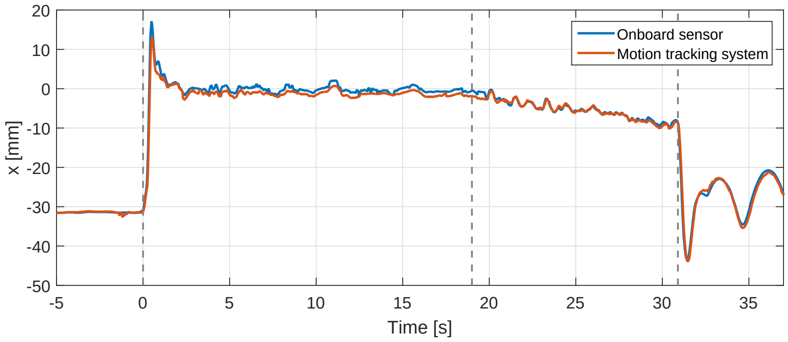

Figure 28: Step response of the controller. Data show the distance between the center of the robot and the center of the payload plate measured by the Vicon motion tracking system and by the onboard sensor. At $t = 0$ s the controller was turned on and the payload plate was held by hand at one place. The controller tries to keep the distance to 0. At $t = 19$ s the plate was released and it was accelerating. The control was turned off at $t = 30.9$ s.

The feedback controller must keep the center of mass of the payload within the area between the air bearings. The air bearings were placed with distance from the center 167 mm on an equilateral triangle. Rubber bumpers were placed conservatively so that this situation was prevented. If the robot's reaction is too slow, the payload touches a bumper and the experiment fails. The closest bumper allows 30 mm clearance.

5.4.2 *Errors*

Figure 26 shows the difference between the expected and measured trajectory of the payload for multiple experiments for an approach velocity of $50\,\mathrm{mm\,s^{-1}}$. The error in the y direction—the direction of the push—is low, below 10 % over the distance of 2 m. Error in the x direction is however significantly higher.

In the x direction, the error is persistent between the experiments and can be explained by a constant acceleration caused mainly by the inclination of the floating plane. As discussed in Section 3, even the slightest inclination of the floating plane results in an acceleration due to the gravity. The inclination during the experiments was mainly caused by the misalignment of the air bearings.

I identified the force in the x direction by fitting the measured error in the experiment with a parabola:

$$\dot{x} = \frac{a}{2}t^2 + v_0 t + x_0$$

where t is the time, a the acceleration, x_0 the initial position, and v_0 the initial velocity.

The fitted curve is shown in Figure 26: the estimated acceleration from the four experiments was $7.24\,\mathrm{mm\,s^{-2}}$ which is below $10^{-3}\,g$. That is a bit higher acceleration than one experienced on the surface of Phobos, see Table 1. The acceleration corresponds to an inclination of around 0.042°.

While the ultimate goal is to run the testbed on ordinary floors, we used the flat floor in the experiments for practical reasons—ORBIT facility was with installed and calibrated Vicon motion tracking system and the experiment was setup there for other platforms, see [26]. However, there was a protective foil which may have impacted the flatness guarantees. As discussed in the next section, in the next iteration of the testbed the height of the air bearings will be automatically adjusted to minimize the error in inclination.

Figure 27 shows that the effect on payload when platform accelerates is unmeasurable as predicted. The payload keeps its velocity even after the acceleration of the platform below.

Overall, it appears that the moving robot has only a negligible effect on the payload and that the main source of the error is from the misalignment of the air bearings.

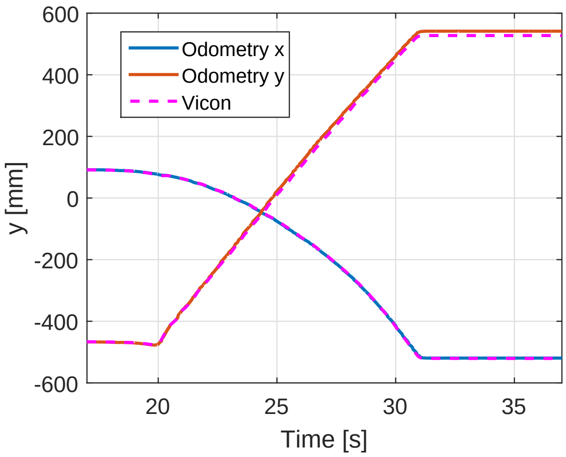

Figure 29: ROOTLESS position during the contact experiment with approach velocity 50 mm s^{-1} from odometric measurements compared to Vicon motion-tracking-system measurement. Slipping was below 2 %.

The data show unexpected torque on floating payload, see Figure 25. It is still pending the analysis to determine the source of the problem.

5.4.3 *Limitations*

The testbed performed well under approach velocities ranging from 20 mm s^{-1} to 100 mm s^{-1}, i.e. under floating velocities ranging from 40 mm s^{-1} to 200 mm s^{-1}. With lower velocities, the acceleration due to inclination dominated. Higher velocities were limited by the maximum acceleration of Youbot, the size of the area between the air bearings, and by the reaction delay in the feedback loop. Further tuning of the PID controller should increase the maximum velocity.

The total weight of the payload with the interface plate attached was 7.64 kg.

6

FUTURE WORK AND CONCLUSIONS

6.1 FUTURE WORK

6.1.1 *Automatic levelling*

The major contribution to the error was the force due to the inclination caused by the misaligned air bearings and by local inclinations of the floor as the robot moves along. While the measured residual acceleration was below $10^{-3}\,g$, the platform will reach its full potential only with integration of the floating-plane automatic levelling.

Automatic levelling requires height adjustment of the air bearings using feedback control as the robot moves and the inclination of the floor changes. Additionally, the floating plane can be tilted to a specific angle so artificial gravity can be introduced as discussed in Section 3.3.

The task is challenging because extremely precise measurement/actuation and fast response are necessary. Given the suitable acceleration on low-gravity bodies like moons or comets, 0.001° precision is required.

This translates into micrometer resolution for actuators with range above 6 mm given the distance between the air bearings on the platform. Linear actuators based on a voice-coil principle seem to be suitable for the task. For instance Voice Coil Positioning Stage VCS06-500-CR-01-MC offers resolution of 1 µm, range of 16.3 mm, and payload of 60 kg with the three actuators.

Ordinary inertial measurement units do not offer this high angular-measurement accuracy and precision. While inclinometers do offer high accuracy, they are based on acceleration measurements and they are suitable for dynamical applications only after data fusion with information from a gyroscope.

The zero angle plane could be calibrated based on the movement of the payload before an experiment and therefore only relative angle measurement is necessary. Gyroscopes are suitable for this. High-end high-precision gyroscopes achieve the required angular accuracy and offer low drift. The drawback could be the high cost and the size as they are mostly used for rocket navigation.

It is easier to accurately measure the angle when the platform is static. One option is to have the robot automatically create an inclination map of the floor before the experiments. Then, during the experiments, the height of the air bearings can be adjusted in open loop based on the map and an accurate 2D-position measurement by, for example, a motion tracking system.

Besides that, an accurate angular measurement can be converted to a less accurate vertical-distance measurement over large horizontal distance. Laser systems are commonly used for the purpose. Using a laser, external reference of the horizon can be provided to the testbed. Several visual sensors on top of the interface plate will measure the height of the reference and from this the angle can be calculated.

6.1.2 *Omnidirectional wheels*

The mechanical design could be further simplified by replacing the current mecanum wheels with omnidirectional wheels specially designed to minimise the gap between the rollers. It would allow to remove the frame with ball transfer units. For instance, [6] proposes such wheel design. Other option may be actuated caster wheels [25].

6.2 CONCLUSIONS

I built and demonstrated a novel testbed for free-floating dynamics. The experiments show that accurate free-floating dynamics even with low-mass objects can be replicated on the testbed.

Comparing to the popular conventional air-bearing platforms, experiments on ROOTLESS are not limited by the size of a flat surface and by the storage of compressed air. Additionally, the limits to the mass of payload and to the velocity of floating are lower. This might make the testbed attractive for research centres and universities as an alternative to air-bearing facilities with flat surfaces.

The mass of the generic interface plate added to the payload was only 2.94 kg. For comparison, the air-bearing platform available at ESTEC weighs more than 27 kg. If the interface surface was specifically designed for the payload, the mass could be even lower.

The main source of error was inclination caused by the misalignment of the air bearings. In the simple experiments, the measured residual acceleration was below $10^{-3}\,g$ using flat floor with a protective foil. This problem will be addressed in the future.

With the promising results, ESA is continuing to develop the concept. In the second iteration of the platform the main upgrade will be the automatic adjustment of the height of the air-bearings to level the floating plane.

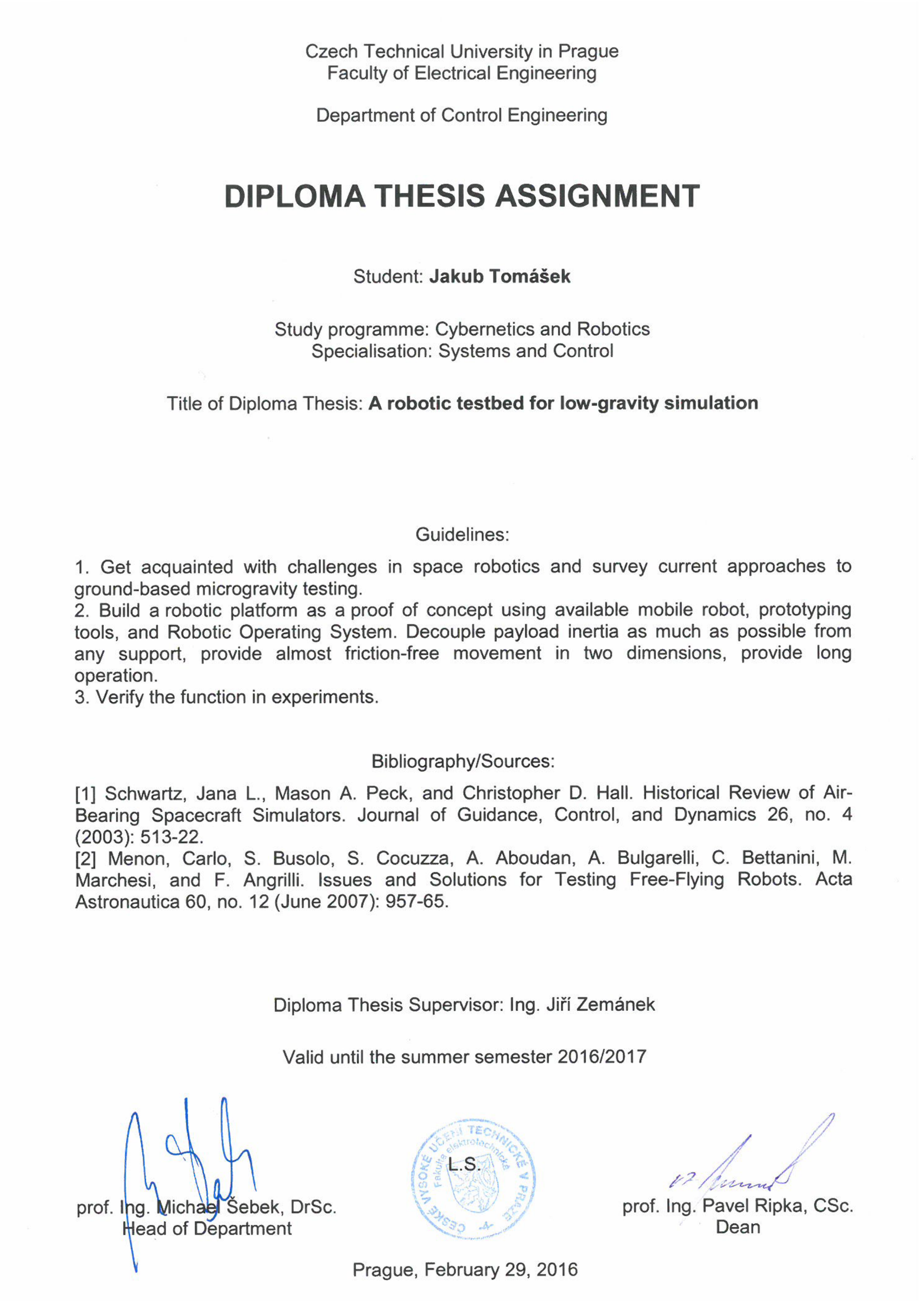

Czech Technical University in Prague
Faculty of Electrical Engineering

Department of Control Engineering

DIPLOMA THESIS ASSIGNMENT

Student: **Jakub Tomášek**

Study programme: Cybernetics and Robotics
Specialisation: Systems and Control

Title of Diploma Thesis: **A robotic testbed for low-gravity simulation**

Guidelines:

1. Get acquainted with challenges in space robotics and survey current approaches to ground-based microgravity testing.
2. Build a robotic platform as a proof of concept using available mobile robot, prototyping tools, and Robotic Operating System. Decouple payload inertia as much as possible from any support, provide almost friction-free movement in two dimensions, provide long operation.
3. Verify the function in experiments.

Bibliography/Sources:

[1] Schwartz, Jana L., Mason A. Peck, and Christopher D. Hall. Historical Review of Air-Bearing Spacecraft Simulators. Journal of Guidance, Control, and Dynamics 26, no. 4 (2003): 513-22.

[2] Menon, Carlo, S. Busolo, S. Cocuzza, A. Aboudan, A. Bulgarelli, C. Bettanini, M. Marchesi, and F. Angrilli. Issues and Solutions for Testing Free-Flying Robots. Acta Astronautica 60, no. 12 (June 2007): 957-65.

Diploma Thesis Supervisor: Ing. Jiří Zemánek

Valid until the summer semester 2016/2017

prof. Ing. Michael Šebek, DrSc.
Head of Department

L.S.

prof. Ing. Pavel Ripka, CSc.
Dean

Prague, February 29, 2016

BIBLIOGRAPHY

[1] Jordi Artigas et al. “The OOS-SIM: An on-ground simulation facility for on-orbit servicing robotic operations.” In: *Robotics and Automation (ICRA), 2015 IEEE International Conference on*. IEEE, 2015, pp. 2854–2860.

[2] J. Biele and S. Ulamec. “Capabilities of Philae, the Rosetta lander.” In: *Space Science Reviews* 138 (2008), pp. 275–289.

[3] Robin Biesbroek, Luisa Innocenti, Stephane Estable, Michael Oswald, Richard Haarmann, Gerrit Hausmann, Carole Billot, and Simona Ferraris. “The e.Deorbit mission: results of ESA’s phase A studies for an Active Debris Removal mission.” In: *66th International Astronautical Congress*. IAC-15,A2,3,4,x30580. International Astronautical Federation. Jerusalem, Israel, 2015.

[4] R. Bischoff, U. Huggenberger, and E. Prassler. “KUKA youBot - a mobile manipulator for research and education.” In: *2011 IEEE International Conference on Robotics and Automation (ICRA)*. 2011.

[5] R. Boumans and C. Heemskerk. “The European Robotic Arm for the International Space Station.” In: *Robotics and Autonomous Systems*. Space Robotics in Europe 23.1–2 (Mar. 1998), pp. 17–27. ISSN: 0921-8890. DOI: `10.1016/S0921-8890(97)00054-7`.

[6] Kyung-Seok Byun, Sung-Jae Kim, and Jae-Bok Song. “Design of continuous alternate wheels for omnidirectional mobile robots.” In: *Robotics and Automation, 2001. Proceedings 2001 ICRA. IEEE International Conference on*. Vol. 1. IEEE, 2001, pp. 767–772.

[7] Elliott Coleshill, Layi Oshinowo, Richard Rembala, Bardia Bina, Daniel Rey, and Shelley Sindelar. “Dextre: improving maintenance operations on the international space station.” In: *Acta Astronautica* 64.9 (2009), pp. 869–874.

[8] Pablo Colmenarejo, Marcos Avilés, and Emanuele di Sotto. “Active debris removal GNC challenges over design and required ground validation.” In: *CEAS Space Journal* 7.2 (2015), pp. 187–201.

[9] H. J. Cruijssen, M. Ellenbroek, M. Henderson, H. Petersen, P. Verzijden, and M. Visser. “The European Robotic Arm: A High-performance Mechanism Finally on Its Way to Space.” In: (2014).

[10] Robert Dedalis and Patrick Mitchell. “Servicing the Hubble - Risk Mitigation, Lessons Learned, and Rewards in Completing Hubble Space Telescope Servicing Missions.” In: *Space 2004 Conference and Exhibit*. American Institute of Aeronautics and Astronautics, 2004.

[11] Fabio Ferrari and Michele Lavagna. “Asteroid Impact Mission: A Possible Approach To Design Effective Close Proximity Operations To Release Mascot-2 Lander.” In: *Proceedings of AIAA/AAS Astrodynamics Specialist Conference*. 2015.

[12] Fabio Ferrari, Michele Lavagna, Marc Scheper, Bastian Burmann, and Ian Carnelli. “The European Asteroid Impact Mission: Phase A Design And Mission Analysis.” In: *Proceedings of AIAA/AAS Astrodynamics Specialist Conference*. 2015.

[13] Angel Flores-Abad, Ou Ma, Khanh Pham, and Steve Ulrich. “A review of space robotics technologies for on-orbit servicing.” In: *Progress in Aerospace Sciences* 68 (July 2014), pp. 1–26. ISSN: 0376-0421. DOI: `10.1016/j.paerosci.2014.03.002`.

[14] Iulia Georgescu. “Rosetta mission: Space oddity.” en. In: *Nature Physics* 12.2 (Feb. 2016), pp. 111–111. ISSN: 1745-2473. DOI: `10.1038/nphys3663`.

[15] Graham Gibbs and Savi Sachdev. “Canada and the International Space Station program: Overview and status.” In: *Acta Astronautica* 51.1–9 (July 2002), pp. 591–600. ISSN: 0094-5765. DOI: `10.1016/S0094-5765(02)00077-2`.

[16] Peter von Kampen, Ulrich Kaczmarczik, and Hans J. Rath. “The new Drop Tower catapult system.” In: *Acta Astronautica* 59.1–5 (2006), pp. 278–283. ISSN: 0094-5765. DOI: `10.1016/j.actaastro.2006.02.041`.

[17] Jun’ichiro Kawaguchi, Akira Fujiwara, and Tono Uesugi. “Hayabusa—Its technology and science accomplishment summary and Hayabusa2.” In: *Acta Astronautica* 62.10–11 (May 2008), pp. 639–647. ISSN: 0094-5765. DOI: `10.1016/j.actaastro.2008.01.028`.

[18] Donald J. Kessler and Burton G. Cour-Palais. “Collision frequency of artificial satellites: The creation of a debris belt.” en. In: *Journal of Geophysical Research: Space Physics* 83.A6 (June 1978), pp. 2637–2646. ISSN: 2156-2202. DOI: `10.1029/JA083iA06p02637`.

[19] Wormnes Kjetil. “Capturing space debris with throw-nets, tethers and harpoons.” In: *CEAS*. Presentation 240. 2015.

[20] Hendrik Kolvenbach and Kjetil Wormnes. “A Facility for Experiments on Free Floating Contact Dynamics.” In: *13th Symposium on Advanced Space Technologies in Robotics and Automation (ASTRA)*. 2015.

[21] Hendrik Kolvenbach and Kjetil Wormnes. “Recent developments on ORBIT, a 3-DoF Free Floating Contact Dynamics Testbed.” In: *13th International Symposium on Artificial Intelligence, Robotics and Automation in Space (i-SAIRAS 2016)*. 2016.

[22] John S. Lewis. “Mining the sky: untold riches from the asteroids, comets, and planets.” In: *Reading, Mass.: Addison-Wesley Pub. Co., c1996.* 1 (1996).

[23] Janice V. Meck, Sherlene A. Dreyer, and L. Elisabeth Warren. “Long-Duration Head-Down Bed Rest: Project Overview, Vital Signs, and Fluid Balance.” In: *Aviation, Space, and Environmental Medicine* 80.5 (May 2009), A1–A8. DOI: `10.3357/ASEM.BR01.2009`.

[24] Alberto Medina, Lorenzo Cercos, Raluca M. Stefanescu, Riccardo Benvenuto, Marco Marcon, Michèle Lavagna, Iván González, Nuria Rodríguez López, and Kjetil Wormnes. “Validation Results of Satellite Mock-Up Capturing Experiment Using Nets.” In: *66th International Astronautical Congress*. IAC-15,A2,3,4,x30580. International Astronautical Federation. Jerusalem, Israel, 2015.

[25] D. Oetomo, Yuan Ping Li, M. H. Ang, and Chee Wang Lim. “Omnidirectional mobile robots with powered caster wheels: design guidelines from kinematic isotropy analysis.” In: *2005 IEEE/RSJ International Conference on Intelligent Robots and Systems*. Aug. 2005, pp. 3034–3039. DOI: `10.1109/IROS.2005.1545385`.

[26] Andrea Pellacani and Hendrik Kolvenbach. “ROSPA, Cross-validation of the platform-art and ORBIT test facilities for contact dynamic scenario setup and study.” In: *6th International Conference on Astrodynamics Tools and Techniques*. ESA/ESOC, 2016.

[27] Morgan Quigley, Ken Conley, Brian Gerkey, Josh Faust, Tully Foote, Jeremy Leibs, Rob Wheeler, and Andrew Y. Ng. “ROS: an open-source Robot Operating System.” In: *ICRA workshop on open source software*. Vol. 3. 2009, p. 5.

[28] Tomasz Rybus and Karol Seweryn. “Planar air-bearing microgravity simulators: Review of applications, existing solutions and design parameters.” In: *Acta Astronautica* 120 (Mar. 2016), pp. 239–259. ISSN: 0094-5765. DOI: `10.1016/j.actaastro.2015.12.018`.

[29] K. Saulnier, D. Pérez, R. C. Huang, D. Gallardo, G. Tilton, and R. Bevilacqua. “A six-degree-of-freedom hardware-in-the-loop simulator for small spacecraft.” In: *Acta Astronautica* 105.2 (2014), pp. 444–462.

[30] Andre Schiele and Jan Smisek. “A New Free Floating Satellite Dynamics Testbed for Hardware-in-the-loop Docking Experiments.” In:

[31] Jana L. Schwartz, Mason A. Peck, and Christopher D. Hall. "Historical review of air-bearing spacecraft simulators." In: *Journal of Guidance, Control, and Dynamics* 26.4 (2003), pp. 513–522.

[32] Raymond Stott, Philippe Schoonejans, Frederic Didot, Cock Heemskerk, and Michel Rog. "Current status of the European robotic arm (ERA), its launch on the Russian multi-purpose laboratory module (MLM) and its operation on the ISS." In: *9th ESA Workshop on Advanced Space Technologies for Robotics and Automation. Noordwijk, Netherlands: ESA/ESTEC*. 2006, pp. 1–7.

[33] Jakub Tomasek, Hendrik Kolvenbach, Marco Pagnamenta, and Kjetil Wormnes. "A robotic testbed for low-gravity simulation." In: *13th International Symposium on Artificial Intelligence, Robotics and Automation in Space (i-SAIRAS)*. Beijing, China, 2016.

[34] Stephan Ulamec et al. "Rosetta Lander–Philae: landing preparations." In: *Acta Astronautica* 107 (2015), pp. 79–86.

[35] P. Verzijden, H. Petersen, and M. Visser. "ERA EQM and FM Test Results." In: *Proceedings of the 7th ESA Workshop on Advanced Space Technologies for Robotics and Automation*. 2000.

[36] P. Verzijden, H. Petersen, and M. Visser. "ERA performance measurements test results." In: *Proceedings of the 7th ESA Workshop on Advanced Space Technologies for Robotics and Automation*. 2002.

[37] Kjetil Wormnes, Ronan Le Letty, Leopold Summerer, Rogier Schonenborg, Olivier Dubois-Matra, Eleonora Luraschi, Alexander Cropp, Holger Krag, and Jessica Delaval. "ESA technologies for space debris remediation." In: *6th European Conference on Space Debris*. ESA/ESOC, 2013.

[38] Kjetil Wormnes, Ronan Le Letty, Leopold Summerer, Rogier Schonenborg, Olivier Dubois-Matra, Eleonora Luraschi, Alexander Cropp, Holger Krag, and Jessica Delaval. "ESA technologies for space debris remediation." In: *6th IAASS Conference:"Safety is Not an Option", Montrel*. 2013.